Solar Flux Dependence of Upper Thermosphere Diurnal Variations: Observed and Modeled

Jeffrey P. Thayer[1], Zachary C. Waldron[1], and Eric K Sutton[2]

[1]University of Colorado Boulder
[2]University of Colorado at Boulder

December 7, 2022

Abstract

Upper thermosphere mass density over the declining phase of solar cycle 23 are investigated using a day-to-night ratio (DNR) of thermosphere properties as a metric to evaluate how much relative change occurs climatologically between day and night. CHAMP observations from 2002-2009, MSIS 2.0 output, and TIEGCM V2.0 simulations are analyzed to assess their relative response in DNR. The CHAMP observations demonstrate nightside densities decrease more significantly than dayside densities as solar flux decreases. This causes a steadily increasing CHAMP mass density DNR from two to four with decreasing solar flux. The MSIS 2.0 nightside densities decrease more significantly than the dayside, resulting in the same trend as CHAMP. TIEGCM V2.0 displays an opposing trend in density DNR with decreasing solar flux due to dayside densities decreasing more significantly than nightside densities. A sensitivity analysis of the two models reveals the TIEGCM V2.0 to have greater sensitivity in temperature to levels of solar flux, while MSIS 2.0 displayed a greater sensitivity in mean molecular weight. The pressure DNR from both models contributed the most to the density DNR value at 400 km. As solar flux decreases, the two models' estimate of pressure DNR deviate appreciably and trend in opposite directions. The TIEGCM V2.0 dayside temperatures during middle-to-low solar flux are too cold relative to MSIS 2.0. Increasing the dayside temperature values by about 50 – 100 K and decreasing the nightside temperature slightly would bring the TIEGCM V2.0 into better agreement with MSIS 2.0 and CHAMP observations.

Solar Flux Dependence of Upper Thermosphere Diurnal Variations: Observed and Modeled

Jeffrey P. Thayer[1,2], Zachary C. Waldron[2], Eric K. Sutton[2]

[1]University of Colorado, Aerospace Engineering Sciences Department, Boulder CO

[2]Space Weather Technology, Research, and Education Center, University of Colorado, Boulder CO

Corresponding author: Jeffrey P. Thayer (jeffrey.thayer@colorado.edu)

Key Points:

- Mass density day-to-night ratio (DNR) from CHAMP observations spanning 2002-2009 increase with decreasing solar flux
- MSIS 2.0 mass density DNR indicate a similar solar flux trend as CHAMP data while TIEGCM V2.0 results display an opposite trend.
- Opposite solar flux trends are revealed in the TIEGCM V2.0 output with TIEGCM dayside temperatures being too cold during middle-to-low solar flux.

Abstract

Upper thermosphere mass density over the declining phase of solar cycle 23 are investigated using a day-to-night ratio (DNR) of thermosphere properties as a metric to evaluate how much relative change occurs climatologically between day and night. CHAMP observations from 2002-2009, MSIS 2.0 output, and TIEGCM V2.0 simulations are analyzed to assess their relative response in DNR. The CHAMP observations demonstrate nightside densities decrease more significantly than dayside densities as solar flux decreases. This causes a steadily increasing

CHAMP mass density DNR from two to four with decreasing solar flux. The MSIS 2.0 nightside densities decrease more significantly than the dayside, resulting in the same trend as CHAMP. TIEGCM V2.0 displays an opposing trend in density DNR with decreasing solar flux due to dayside densities decreasing more significantly than nightside densities. A sensitivity analysis of the two models reveals the TIEGCM V2.0 to have greater sensitivity in temperature to levels of solar flux, while MSIS 2.0 displayed a greater sensitivity in mean molecular weight. The pressure DNR from both models contributed the most to the density DNR value at 400 km. As solar flux decreases, the two models' estimate of pressure DNR deviate appreciably and trend in opposite directions. The TIEGCM V2.0 dayside temperatures during middle-to-low solar flux are too cold relative to MSIS 2.0. Increasing the dayside temperature values by about 50 – 100 K and decreasing the nightside temperature slightly would bring the TIEGCM V2.0 into better agreement with MSIS 2.0 and CHAMP observations.

Plain Language Summary

The mass density of the upper thermosphere varies daily as the atmosphere thermally expands and contracts due to dayside heating and nightside cooling, respectively. However, the magnitude of change in mass density from day-to-night is not well described. The general consideration is that this day-night ratio (DNR) in mass density is constant regardless of solar flux levels. This study demonstrates through observations and modeling that the mass density DNR varies from a value of two during solar maximum to a factor of four during solar minimum. This has implications on how the thermosphere responds to geomagnetic storms under these two phases of the solar cycle, and the level of drag a spacecraft in low Earth orbit will experience. The cause of such change is suggested to lie within the thermosphere itself by how solar energy is transformed and transported globally. Simulations from a physics-based model suggests the dayside thermosphere during solar minimum requires higher temperatures to better represent the observations. Several

mechanisms are possible that could alter the model's dayside and nightside temperatures, but further investigation is required to identify any one mechanism as the cause.

1 Introduction

The description of neutral mass density structure in the thermosphere has improved significantly over the past two decades with the advancement of scientific-grade accelerometers sensitive to nano-G forces. These observations are capable of deriving thermosphere neutral mass density and neutral winds at high-resolution (< 100 km) along the orbital track (e.g., Bruinsma et al., 2004; Doornbos et al., 2010; Sutton, 2008; Sutton et al., 2007). The Challenging Minisatellite Payload (CHAMP) and Gravity Recovery and Climate Experiment (GRACE) missions, whose measurements spanned 2000-2010 and 2002-2014, respectively, continue to be important sources of data for analysis, validation, and assimilation. Several reviews of thermosphere mass density structure and behavior have resulted from these data sets (e.g., Qian & Solomon, 2012; Stolle & Liu, 2014 ; Emmert, 2015). Qian & Solomon (2012) summarize the many variations, observed and modeled, in thermosphere density and attribute these variations to several driving mechanisms, including extreme ultraviolet (EUV) solar flux. Emmert (2015) reviews thermosphere density spatial and temporal behavior spanning the period from 2000 to 2014 with features and processes categorized as either climate (time-independent or slowly varying) or weather (time-dependent or quickly varying) phenomena. These reviews will serve as guideposts to this study's targeted investigation.

Here, diurnal variations in the upper thermosphere from observations and models are investigated over the declining phase of solar cycle 23 under quiet geomagnetic conditions to investigate climatologically how the dayside structure relative to the nightside structure in mass density (and a few other properties) at 400 km altitude changes with the level of EUV solar flux. The purpose for such a study is multifold. The first is to establish the day-to-night changes in mass density experienced by a low Earth orbiting spacecraft for a given level of solar flux. The relative change between day and night densities will affect the drag force along the orbit and the orbit energy dissipation rate over time. The second purpose is to establish the preconditioned state of the thermosphere during quiet times for specific solar flux levels to properly predict the thermosphere response to geomagnetic activity. It can be demonstrated that the relative change in mass density for a warm thermosphere will be less than the relative change for a cold thermosphere given the same energy input into the system. This occurs because the perturbed density is an integrated response to changes in temperature, to first order. With the same energy input, the perturbation in temperature will constitute a larger fraction of the total temperature for a colder thermosphere. This results in a larger change in density scale height and a greater relative change in mass density for a given altitude. Consequently, knowing and understanding the preconditioned state of the dayside relative to the nightside density will provide a better understanding of how mass density at a fixed altitude will respond globally to geomagnetic activity. Finally, taking a ratio of day and night density values from CHAMP observations alleviates concerns about the absolute calibration of the measurements.

A day-to-night ratio (DNR) of thermosphere properties is used in this paper as a metric to evaluate how much relative change occurs between day and night for different levels of solar flux. CHAMP observations from 2002-2009 are used to construct the mass density DNR from every orbit with specific binning criteria described in Section 3. Thermosphere mass density and temperature DNRs from model simulations at similar altitudes as CHAMP are also determined over the same observing period to compare with the observations and to assess the sensitivity of the models to EUV solar flux changes in terms of day-night changes in thermosphere properties.

The daytime increase and nighttime decrease in density at a fixed altitude of 400 km is a regular feature in the CHAMP data set and, to first order, is observed to be highly correlated with proxies of EUV flux (e.g., Guo et al., 2007). Yet, there are few studies that have investigated how the two opposing states of the thermosphere (dayside maximum and nightside minimum) trend with each other under changing solar EUV flux levels. Müller et al. (2009) investigated the thermosphere mass density DNR from CHAMP measurements collected from 2002-2005. Conclusions from that study suggested the mass density DNR was near a value of two and did not change much with solar flux or season over this four-year period. Qian & Solomon (2012) presented results from a National Center for Atmospheric Research Thermosphere-Ionosphere Electrodynamics General Circulation Model (NCAR-TIEGCM, henceforth referred to as TIEGCM) simulation over several days in 2007 with day and night thermosphere mass density behavior at 400 km altitude also displaying a factor of 2 in their ratio. However, Emmert (2015) indicated that the maximum dayside density is typically 3.5 times larger than the minimum night side density. Is a fixed ratio between day and night thermosphere mass density under changing solar flux an expected result or should there be a dependence on solar flux levels given its dominating influence on the thermosphere neutral gas? This question is addressed in this study using CHAMP data that spans eight years of change in the solar climate with EUV flux values steadily decreasing during the declining phase of solar cycle 23. The observed behavior is compared with NRLMSIS 2.0 output (Emmert et al., 2021, henceforth referred to as MSIS 2.0) and TIEGCM V2.0 simulations using the DNR metric to assess their relative response to the same change in solar flux as the observations.

Early studies of the thermosphere assumed that EUV heat input and vertical conduction of heat were entirely responsible for setting up the diurnal structure of the thermosphere (e.g., Harris & Priester, 1962; Nicolet, 1961). This led to a discrepancy that Harris & Priester (1965) attempted to represent in their one-dimensional model of thermospheric heating and dynamics with an anomalous “second heating source”. Evidence of an influence on the diurnal thermal structure from the global neutral circulation was suggested after analyzing two-dimensional models (radial and zonal) of Dickinson et al., (1968) and Volland (1969). The lateral transport of neutral species was studied by Johnson & Gottlieb (1970), and Reber & Hays (1973), with recent additions by Sutton (2016). Further attention was given to the influence of ion-neutral collisions on this global neutral circulation (Mayr & Volland, 1973) with more recent attention to drag effects on the diurnal thermosphere structure provided by Hsu et al. (2016) using TIEGCM V2.0.

In essence, the behavior in thermosphere mass density is a complex collection of thermal and constituent transport that varies with altitude, local time, latitude, season, and solar flux / geomagnetic conditions. The local-time phase anomaly between temperature and mass density maxima on the dayside at 400 km altitude is a demonstration of this complexity (Hedin et al. 1978; Mayr & Volland 1973). Explanations for mass density peaking an hour or so earlier than temperature on the dayside invoke adiabatic cooling and departures from diffusive equilibrium and dynamical transport of thermosphere constituents below 200 km (Mayr & Harris 1977), whereby lighter constituents gather at earlier local times. These effects leave an imprint on the mass density structure at higher altitudes and cause a dayside local-time lag between mass density and temperature at 400 km

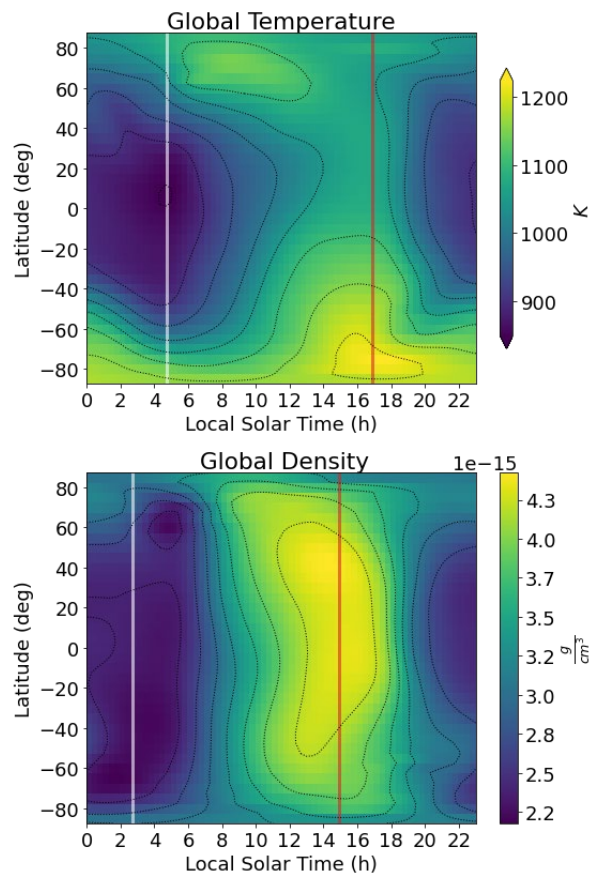

Figure 1. Latitude-local time contour plot of temperature (top) and mass density (bottom) at 400 km from TIEGCM simulation for the 2003 March Equinox at 12 UT with low-geomagnetic activity. The approximate local-time peak and trough in each atmospheric property is marked with a vertical red line and white line, respectively.

altitude, see Figure 1 from a TIEGCM V2.0 simulation. A similar daytime lag in local time is found in MSIS 2.0, with the dynamical transport in the lower atmosphere being approximated by prescribed composition fields. Consequently, we must lean on physics-based simulations to implement the processes and use observations to validate the output. While many of the early studies listed here focused on changes over the course of a day, our investigation is focused on the diurnal amplitude of the thermosphere mass density change, using the DNR metric, over long-term changes in solar flux using CHAMP observations, MSIS 2.0 output, and TIEGCM V2.0 simulations. The physics-based modeled DNR can provide additional insight as its value results from processes associated with redistributing solar EUV flux energy input through coupled thermodynamics, hydrodynamics, and mass continuity processes.

This paper will focus on the climatological response of thermosphere DNR properties from solar maximum to solar minimum. Organization of the data will minimize “weather features” to give a more robust climatological description of the preconditioned DNR. Section 2 provides a description for interpreting the mass density DNR at a fixed altitude. Section 3 describes the CHAMP data source and the use of MSIS 2.0 and TIEGCM V2.0 in the study. Section 4 describes data handling methods and the approach used to construct the DNR. Section 5 analyzes the DNR from CHAMP and performs data-model-model comparisons followed by more general model-model comparisons between MSIS 2.0 and TIEGCM V2.0. Section 6 discusses the results and evaluates the mass density DNR produced by the TIEGCM. The results and summary of findings are described in Section 7.

2 Thermosphere Mass Density Day-to-Night Ratio at Fixed Altitude

Interpreting mass density change at a fixed altitude (or normalized to a fixed altitude as in the CHAMP data) is challenging because pressure, temperature, and composition changes that lead to mass density change are coupled. If on a constant pressure surface, temperature and composition changes are separable from each other. That is one of the reasons why it is common practice to represent mass density change on constant pressure surfaces in physics-based models. Lei et al. (2010) describes and illustrates the differences of interpretation on a fixed altitude and a constant pressure surface for a storm-time investigation of thermosphere mass density change. Here, we will describe the approach for interpreting the day-to-night behavior in thermosphere mass density

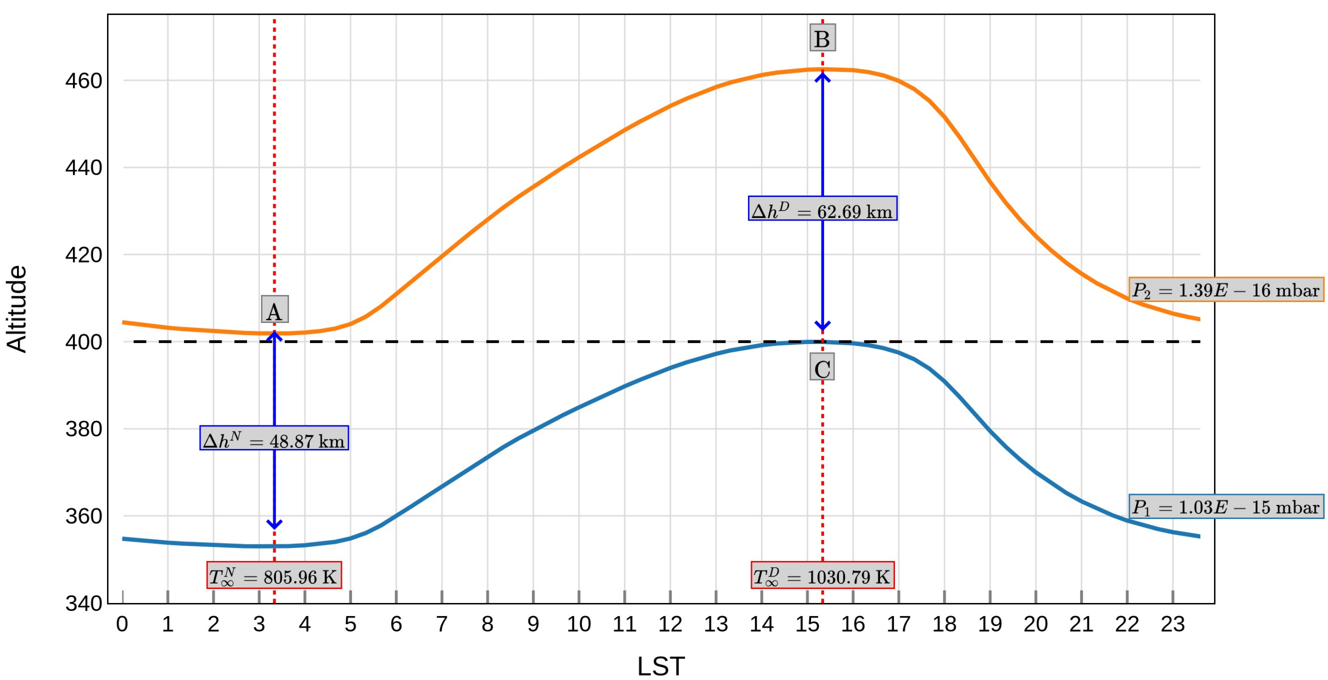

Figure 2. A schematic showing two pressure levels from TIEGCM output at 12 UT projected onto geometric altitude versus local solar time. The depicted pressure lines from TIEGCM are selected by locating the pressure level closest to 400 km at night and day after averaging over ±40° latitude band. An $F_{10.7}$ value of 120 was used.

at a fixed altitude under quiet conditions.

Figure 2 is a schematic diagram of two pressure surfaces near the 400 km altitude level over 24 hours in local solar time from output of the TIEGCM. One pressure surface (P_1) equals the pressure at 400 km altitude (C) at ~15 local time while the other surface represents a lower pressure (P_2) at 400 km altitude at ~03 local time (A). These local times closely, but not exactly, represent the dayside maximum (D) and nightside minimum (N) in thermosphere mass density, respectively. The exospheric temperature for each of these local times is indicated as T_∞^N and T_∞^D, and it is assumed that these temperatures apply over the altitude range depicted. An additional point (B) is indicated to lie at the same local time as (C) but on the lower-valued pressure surface (P_2) that includes point (A).

Given (A) and (B) are on the same pressure surface (P2) but different local times and by applying the ideal gas law,

$$\rho_2^D = \rho_2^N \frac{T_\infty^N}{T_\infty^D} \frac{\bar{m}_2^D}{\bar{m}_2^N} \tag{1}$$

where ρ_2 and $\bar{m}_2$ are the mass density and mean molecular weight on the P_2 pressure surface. The superscript N represents the 03 local time of the nightside density minimum, and D represents the 15 local time of the dayside density maximum at 400 km altitude. This relation illustrates the benefit of interpreting mass density change on constant pressure surfaces. On a constant pressure surface, altering the mass density through a change in the composition mixing ratio requires either transport or a chemical production / loss process to occur. Thermal changes are the other means to alter mass density on a constant pressure surface (an increase in temperature results in a decrease in density on a constant pressure surface).

The pressure surface, P_1, crosses the 400 km altitude line at point C and, using the hydrostatic relation and the definition of Z used in the TIEGCM, is related to the pressure surface at point B (P_2) by

$$P_1 = P_2 \exp(\Delta Z) \quad where \quad \Delta Z = Z_2 - Z_1 \quad and \quad Z = -7 + \int_{h_0}^{h} \frac{dh}{H} \tag{2}$$

where h is the altitude variable and H is the pressure scale height. Using the ideal gas law,

$$\rho_1^D = \rho_2^D \frac{\bar{m}_1^D}{\bar{m}_2^D} \exp(\Delta Z) \tag{3}$$

Substituting the daytime density at pressure level P_2 from (1) into (3) results in

$$\rho_1^D = \rho_2^N \frac{\bar{m}_1^D}{\bar{m}_2^N} \frac{T_\infty^N}{T_\infty^D} \exp(\Delta Z) \tag{4}$$

The daytime values on the P_1 surface are the same daytime values at 400 km altitude and the nighttime values on the P_2 surface are the nighttime values at 400 km altitude – see Figure 2. Therefore, equation (4) can be expressed in terms of constant altitude as,

$$\rho_{400}^D = \rho_{400}^N \frac{\bar{m}_{400}^D}{\bar{m}_{400}^N} \frac{T_\infty^N}{T_\infty^D} \exp(\Delta Z) \tag{5}$$

Furthermore, day-to-night ratios at a constant altitude can be used to rearrange equation (5) as,

$$\frac{\rho_{400}^D}{\rho_{400}^N} = \frac{\bar{m}_{400}^D}{\bar{m}_{400}^N} \frac{T_\infty^N}{T_\infty^D} \exp(\Delta Z) \tag{6}$$

Finally, the change in Z between points C and B, i.e., ΔZ, is the same value as the change in Z between daytime point C and nighttime point A at 400 km resulting in a day-to-night pressure ratio producing perhaps the intuitive result,

$$\frac{\rho_{400}^D}{\rho_{400}^N} = \frac{\bar{m}_{400}^D}{\bar{m}_{400}^N} \frac{T_\infty^N}{T_\infty^D} \frac{P_{400}^D}{P_{400}^N} \quad or \quad \rho_{DNR} = \bar{m}_{DNR} \frac{P_{DNR}}{T_{DNR}^\infty} \tag{7}$$

This construct for the mass density DNR will be used in the interpretation of TIEGCM results in Section 6.

3 Data Sources and Models

3.1 CHAMP Satellite Observations

The density measurements used in this paper are from the version 2.3 release of the CHAMP accelerometer-derived atmospheric densities normalized to 400 km altitude provided by Sutton, (2009). The CHAMP satellite was launched into a near-polar, nearly circular orbit on July 15, 2000 until the mission ended on September 19, 2010. The high-latitude orbit has an inclination of 87.3°, which allows almost complete latitudinal coverage at two different local times during its orbit around the globe. On any given day, the satellite orbits the earth 16 times, sampling a multitude of longitudes, but only two distinct local times. CHAMP precesses to earlier local times at a rate of 12 LST hours every 133 days.

Figure 3a shows an arbitrary day of the CHAMP orbit over twenty-four hours. The left panel shows the ground tracks plotted with respect to latitude and longitude while the right panel shows the ground tracks with respect to latitude and local time. Figure 3b illustrates the CHAMP altitude over the period of the study. The CHAMP data from 2002 through 2009 are used in this study to cover the period of solar maximum to solar minimum. From its initial altitude at 456 km, CHAMP's orbital altitude decayed to 400 km by 2004, and to 310 km by 2010.

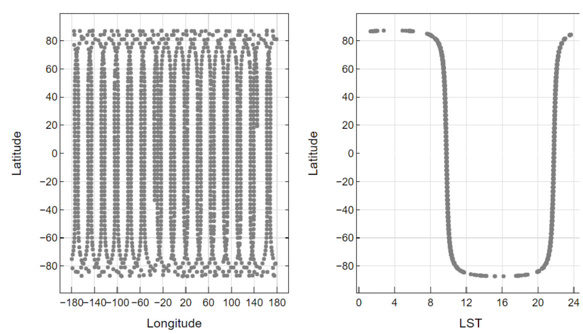

Figure 3a. Longitudinal (left) and local solar time (right) coverage of the CHAMP satellite over the 2003 spring equinox.

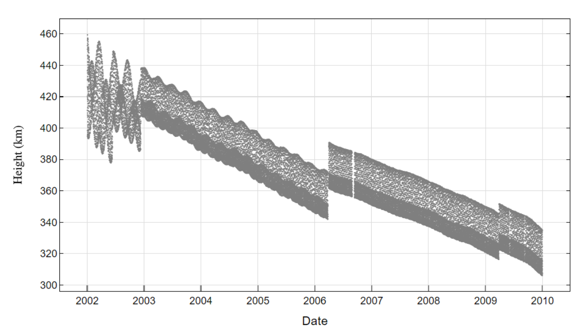

Figure 3b. Geometric altitude of the CHAMP satellite from 2002 through 2009.

3.2 TIEGCM

The TIEGCM V2.0 used in this study is described comprehensively by Qian et al. (2014). The model datasets used in this research have a grid resolution of 5° x 5° in latitude and longitude and a time resolution of 120 seconds. Model output is interpolated to the CHAMP orbital track to best represent the observations. A description of the interpolation process to the CHAMP orbital track is provided in Figure 4.

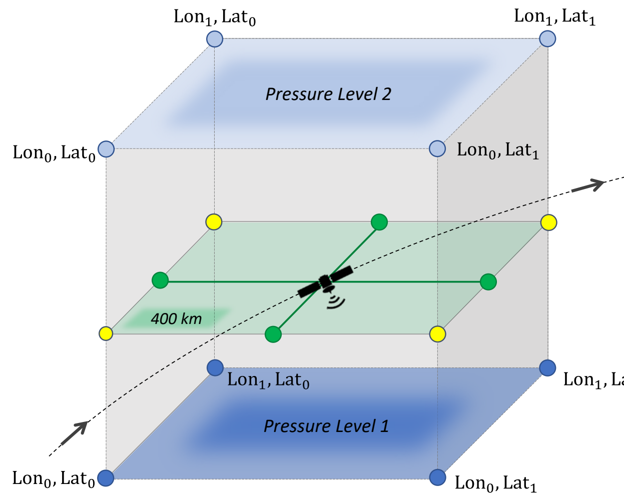

Figure 4. A schematic showing the trilinear interpolation process used to sample the TIEGCM model along the CHAMP orbital track. The density interpolation from pressure levels (blue grids) to geometric altitude (green grid) is done in log space. Interpolation is done along each vertical column such that the densities are interpolated from the blue points to yellow points to green points, and finally to the satellite position.

To span the seven years of observations, the model is driven by the magnesium II core-to-wing ratio (MgII) index, which has a very high correlation to $F_{10.7}$ (shown in section 3.1.4) and serves to enhance the accuracy of the model during times of deep solar minimum (Kodikara et al., 2019; Thuillier & Bruinsma, 2001). While discrepancies between the $F_{10.7}$ index and MgII index do exist (Thuillier & Bruinsma, 2001; Viereck et al., 2004), they primarily occur under low solar minimum conditions where MgII is the preferred index for the EUV proxy in the TIEGCM (Solomon et al., 2011). This is further reinforced by (Viereck et al., 2004) which showed that F10.7 exhibits less accuracy in times of solar minimum relative to MgII. Daily runs of the TIEGCM V2.0 model were constructed for the period of interest from 1 January 2002 through 31 December 2009. Each simulation was run using the same input specifications. A spin-up period was used in advance of the period of interest to allow TIEGCM to converge towards a stable simulation. File-based simulation histories were used as model inputs where necessary, such as between changing years, to allow continuity.

3.3 MSIS 2.0

The MSIS 2.0 model is employed to provide the empirical description of thermosphere mass density and temperature. The model output at 400 km is determined by providing the MgII scaled, observed daily F10.7 (and its 81-day average) and geomagnetic activity over the seven-year data window along with position and time. The MSIS 2.0 mass density and temperature are used in the analysis of the DNR over the span of the observations. The MSIS 2.0 model is accessed via the Pymsis python module (Lucas, 2021; Emmert et al., 2021).

4 Methods

4.1 Data Handling and Selection Criteria

A dayside and nightside collection window in latitude and local time is constructed to organize the data. MSIS 2.0 is used for global representations of the dayside and nightside densities and to aid in our defining of the local solar time (LST) and latitude criteria. Once established, all three sources of data are organized the same way. Given the climatological nature of MSIS 2.0, the output has been used as a general guide to establish the range in local time and latitude required to capture the dayside mass density maximum and the nightside minimum.

4.1.1 Local Solar Time

Figure 5 provides a representative description of mass density contours for day of year 172 in 2004 at 12 UT from output of MSIS 2.0. The colored regions highlight the latitude and local time ranges that ensure the dayside maximum (green region) and nightside minimum (blue region) lie within. Figure 5 shows

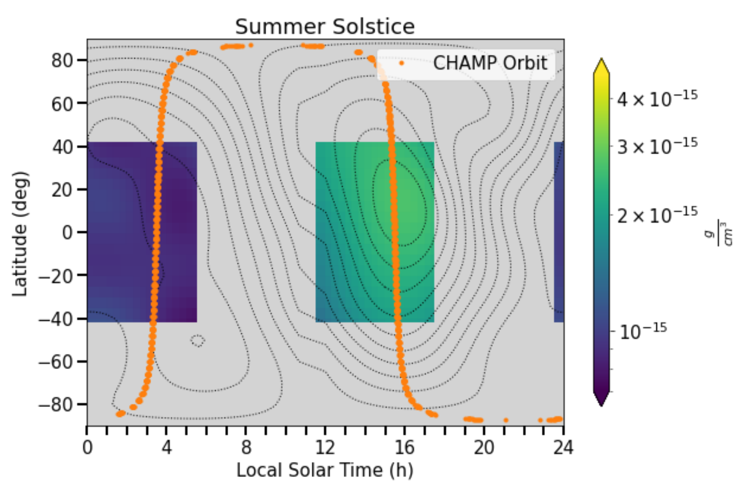

Figure 5. Visualization of local time and latitude selection criteria is displayed. The dayside (green, 11.5 – 17.5 LST) and nightside (violet, 5.5 - 23.5 LST) criteria windows are superimposed over an MSIS 2004 summer solstice mass density field. The CHAMP orbital track is overlaid in orange.

the CHAMP satellite orbit in local time and latitude as an orange ground track for this particular day in 2004, offering a visualization for both the selection criteria and how the satellite orbit would sample the region in MSIS 2.0. Centering the local-time windows around the dayside peaks and nightside troughs limits the local time bias in the day-to-night ratio of mass density that would otherwise arise as the satellite precesses over the local-time windows. The determined local-time window is 11.5 – 17.5 LST hours on the dayside and 5.5 - 23.5 LST hours on the nightside. This is shifted 1-hour later in the day relative to the windows used by Müller et al. (2009).

4.1.2 Latitude and Longitude

To capture the density peak in the latitude dimension, the data window spans ±40° latitude. This is 10° wider than the latitude window used by Müller et al. (2009). The nightside trough in density is less centralized than that of the dayside density peak, so widening the window in the latitudinal dimension offers better coverage of the nightside density. Within the latitude window, the dayside and nightside density values are averaged into 3° latitude bins. The day-to-night ratio is then computed for each latitude bin. In a single day, the satellite samples two different local times while the Earth rotates below it (shown by the orange ground tracks in Figure 5). This results in evenly distributed coverage across all longitudes. Since the average is taken with respect to latitudes, and there is consistent longitudinal coverage in a single day, any variation in longitude is smoothed out through the averaging process.

4.1.3 Geomagnetic Activity

Geomagnetic storms cause transient increases in the neutral mass density, creating perturbations in the dayside and nightside density that would be present in the day-to-night ratio making it difficult to interpret the solar flux effects. Thus, only geomagnetically quiet times with Ap less than 15 are included. The Ap values are taken from the NOAA archive.

4.1.4 Solar Flux

At the beginning of our time of interest, 2002, the sun is in the maximum EUV flux portion of solar cycle 23. At the end of the period, the sun has fully entered deep solar minimum. Figure 6 shows the $F_{10.7}$ solar flux for our period of interest. The blue curve is the daily measured value of $F_{10.7}$ from the Ottawa observatory. The green curve is the MgII index, computed by scaling the $F_{10.7}$ values with the MgII core-to-wing ratio. All MSIS2.0 and TIEGCM simulations presented use the MgII index.

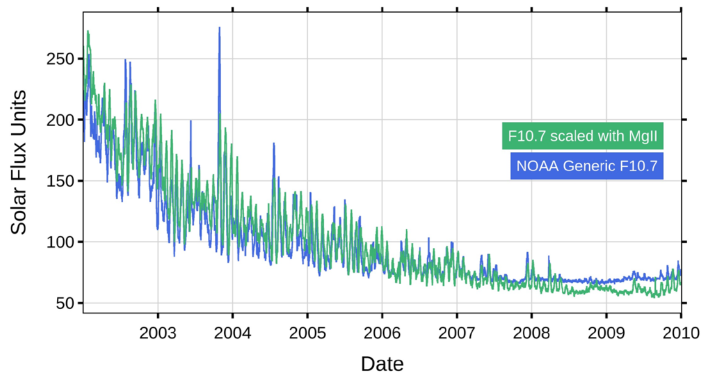

Figure 6. Proxy indicators of solar EUV flux with standard $F_{10.7}$ in blue and scaled $F_{10.7}$ by MgII in green.

4.1.5 Season

Owing to the local time window and the satellite precession, certain parts of the year are void of DNR data – see Figure 5. There are three intervals per year, each lasting about 60 days, where the satellite is not passing through the prescribed local-time window. Over the seven years, these intervals move through the seasons with a repeated pattern every four years. Due to the satellite sampling and local time window criteria, seasonal variations will be mixed within these CHAMP DNR estimates.

5 Analysis – Constructing the Day-to-Night Ratio

The criteria for constructing the day-to-night ratio from CHAMP data were described in detail in Section 3.2.1. and are applied to the dayside and nightside densities to compute day-to-night ratios in this section. A summary of the criteria is: 1) dayside window: 11.5 − 17.5 LST, 2) nightside window: 23.5 − 5.5 LST, 3) days with low Ap values (Ap < 15), and 4) low latitudes (± 40°). These criteria are applied to the CHAMP dataset from 2002-2009.

5.1 CHAMP DNR

The process for producing the day-to-night ratio for a single day of CHAMP data is described here and subsequently applied to all days from 2002-2009. The top panel of Figure 7 shows the density for a single day of CHAMP data from the 2004 summer solstice. The CHAMP satellite orbits the earth about 16 times in a day, which accounts for the oscillation in the density as the satellite passes through the day and night local time sectors. The density values have been normalized to 400 km to eliminate any altitudinal dependence caused by the slightly eccentric CHAMP orbit and the decreasing altitude of CHAMP over the observing period. The top panel of Figure 7 shows all densities in gray values without any criteria applied. The middle panel depicts the local-time selection criterion acting on the data such that the dayside (11.5 - 17.5 LST) and nightside (23.5 - 5.5 LST) portions of the values are identified by their respective colors. The bottom panel of Figure 7 shows the effects of applying the latitude selection criterion such that chosen densities are within ±40° latitude.

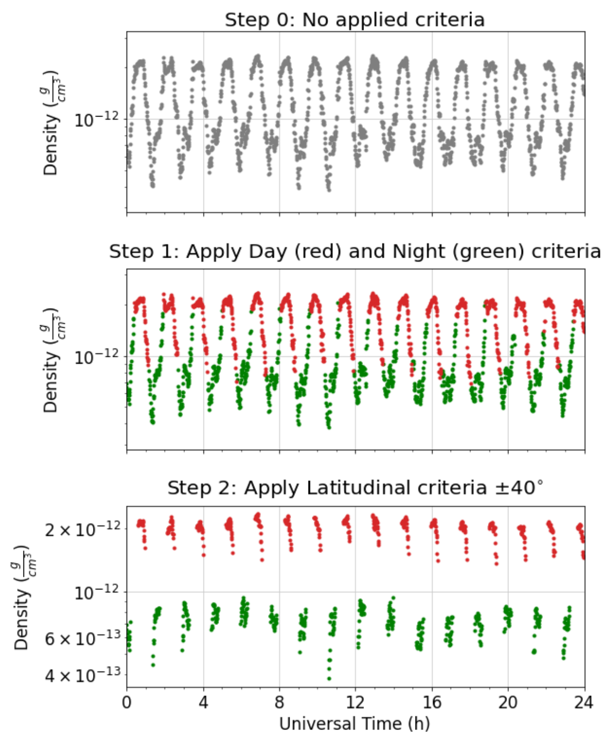

Figure 7. Top panel: CHAMP density data for 2004 summer solstice with no criteria applied. Middle panel: CHAMP density selected according to local time values, dayside (red, 11.5 - 17.5 LST) and nightside (green, 23.5 - 5.5 LST). Bottom panel: CHAMP density selected with both local time and ± 40° latitude criteria applied.

Next, the dayside and nightside values are averaged within 3° latitude bins, resulting in 29 dayside and 29 nightside averages of mass density per day. The effects of averaging the latitude bins are shown in the top panel of Figure 8, which plots average density against latitude. Now that we have binned averages at each dayside and nightside latitude range, we can take the ratio with respect to each latitude bin and get a value of the mass density day-to-night ratio at each represented latitude, shown in bottom panel of Figure 8. For the purposes of constructing a time series, the dayside times are stored and averaged, and the day-to-night ratios are assigned to these times.

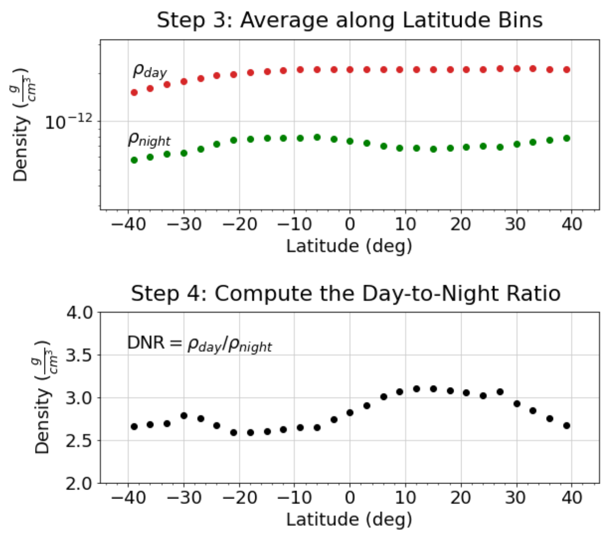

Figure 8. Top panel: CHAMP density from Figure 7 averaged within 3° latitude bins. Bottom panel: Day-to-night ratios computed for each 3° latitude bin.

Figure 9 depicts the dayside and nightside mass densities of CHAMP at 400 km altitude for the period of interest (2002-2009), and their subsequently determined DNR. The top panel of Figure 9 shows the dayside and nightside densities without applying the DNR criteria. The middle panel shows dayside (orange) and nightside (blue) mass densities with the criteria applied. The bottom panel shows the mass density day-to-night ratios as determined when the criteria are applied to the CHAMP satellite data. Explicitly stated, this plot is the result of dividing the middle plot's dayside value (orange curve) by the nightside value (blue curve). Due to the limited local-time sampling of the CHAMP satellite, and its 12-hour local-time precession every 133 days, the data becomes decimated as the satellite precesses out of the dayside and nightside local-time criteria windows.

This causes large gaps that appear ~3 times every year in the middle and bottom panels. The sampling also causes each continuous observing period to have an arch-like shape. This is expected as the local-time sampling of the satellite approaches and then passes through the maximum DNR over the course of its precession through the local-time window. Similar arch-like patterns will be seen in the satellite-sampled model output as well.

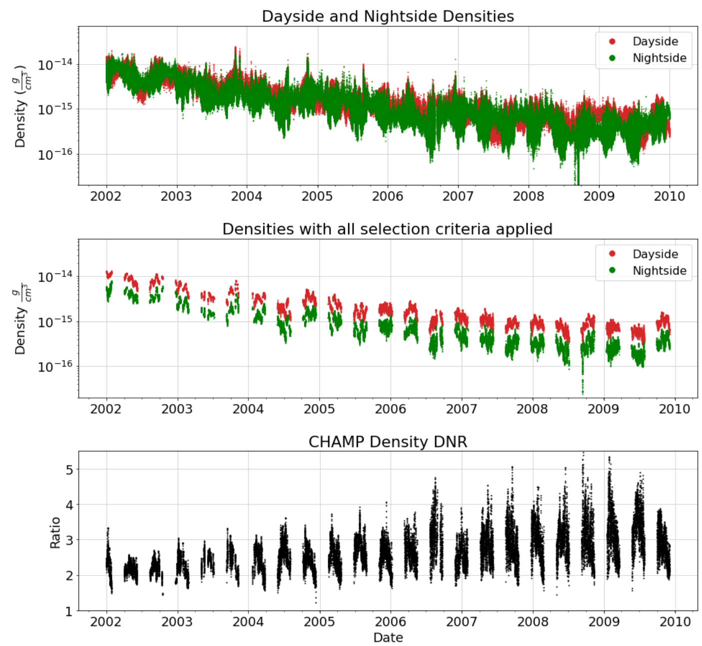

Figure 9. Top panel: CHAMP dayside and nightside densities normalized to 400 km over all study years with only the local time criteria applied. Middle panel: Normalized CHAMP dayside and nightside densities with all criteria applied for all study years. Bottom panel: CHAMP density day-to-night ratio with all criteria applied and for all study years.

Most notable in the lower panel of Figure 9 is the trend that is present in the CHAMP mass density DNR with solar flux. The mass density DNR increases with respect to decreasing solar flux (noting from Figure 6 that the solar flux steadily decreased throughout the entire period of interest). The DNR values range from 2.5 during solar maximum to 4.5 in solar minimum with some fluctuation between collection periods that may be due to season. These results are in stark contrast to the results put forth by Müller et al. (2009), specifically in their Figure 4. They find that the timeseries of the day-to-night ratio in CHAMP is independent of solar flux levels and seasonal variation, although their study did contain only four years near solar maximum (2002-2005). Extending the parameters of this study to include the complete declining phase of solar cycle 23 shows a significant increase in the day-to-night ratio of almost 1.5 times the ratio that is determined near 2005.

The normalization of the CHAMP density to 400 km altitude performed in Sutton (2011) was evaluated to assess the influence of the background model on DNR trends. The data presented in Figure 9 were normalized using MSIS as the background model, per Sutton (2009). The density normalization was also tested using the TIEGCM V2.0 as the background model. This resulted in a shallower DNR trend but nonetheless produced an increasing DNR value with decreasing solar flux. It will be shown that the TIEGCM produces the opposite trend in DNR behavior as observed and so is likely not the appropriate model to use in normalizing the satellite data over this period.

5.2 Data-Model-Model DNR Comparison

The method to produce day-to-night ratios is extended to the atmospheric models to see how they capture this metric relative to the CHAMP data. This provides inter-model and model-to-observation comparisons, both for the sake of assessing discrepancies, as well as to provide additional physical context that may aid in our understanding of the mass density DNR behavior with solar flux. The MSIS 2.0 and TIEGCM V2.0 models are sampled with the CHAMP satellite ephemeris by “flying” the satellite through the modeled atmosphere and indexing the physical properties of the model at the time and location of the satellite. The sampled densities for each model undergo the same selection criteria and methodology as described in Section 4.1 when constructing the dayside and nightside densities and the

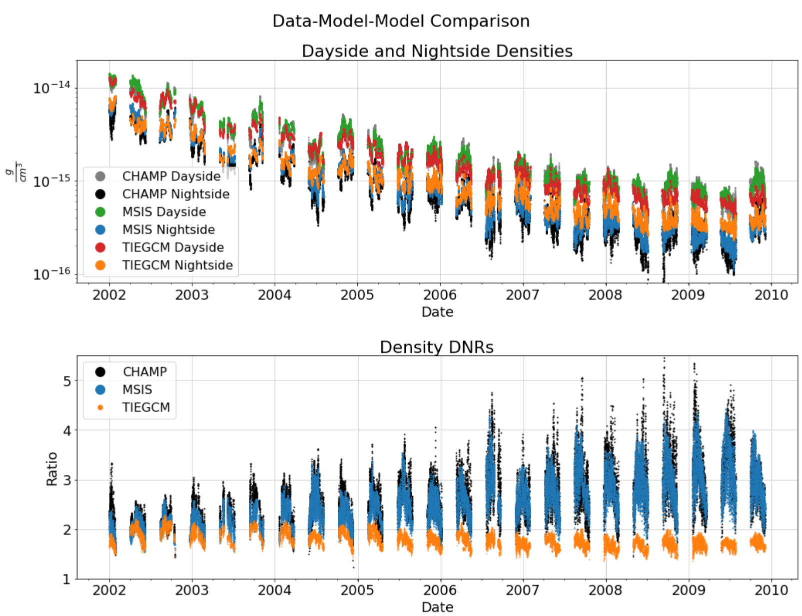

Figure 10. Top panel: Densities with all selection criteria applied using the following color scheme: CHAMP dayside (gray) and CHAMP nightside (black), MSIS dayside (green) and MSIS nightside (blue), TIEGCM dayside (red) and TIEGCM nightside (orange). Bottom panel: Mass density day-to-night ratios for the CHAMP data (black), the MSIS 2.0 model (blue), and the TIEGCM model (orange).

day-to-night ratios. A comparison of these results is shown in Figure 10. The top panel of Figure 10 shows the criteria-applied dayside and nightside densities on a log-scale as estimated by MSIS 2.0 and TIEGCM along the orbit of CHAMP and compares them to observed measurements from CHAMP over the eight-year period. The bottom panel shows the MSIS 2.0, TIEGCM, and CHAMP respective mass density day-to-night ratios. Observed values from CHAMP are in black, MSIS 2.0 sampled data are in blue, and TIEGCM sampled data are in orange. The same arch-like shape observed in the data is present in the sampled model output. While MSIS 2.0 values follow the trend seen in CHAMP (increasing DNR as solar flux decreases), the TIEGCM values depict an opposing trend with decreasing DNR as solar flux decreases.

The dayside and nightside densities in the top panel of Figure 10 offer some supplementary insight into the day-to-night ratio results shown in the bottom panel. Overall mass density values from all three sources of data decrease with solar flux, but the relative decrease of dayside and nightside values differ between data sources. As solar flux decreases, the CHAMP observed nightside densities decrease more significantly than the decrease in CHAMP dayside density. This causes an increase in the CHAMP mass density DNR with decreasing solar flux. The MSIS 2.0 dayside and nightside densities decrease less than those of CHAMP, but the nightside densities decrease more significantly than the decrease in dayside density, resulting in the same trend as CHAMP of increasing DNR with decreasing solar flux. An opposing, decreasing trend of DNR seen in TIEGCM V2.0 output is due to dayside densities decreasing more significantly than nightside densities with decreasing solar flux.

5.3 Model-Model DNR Comparison

The mass density DNR provides a means to assess climatologically a model's ability to globally construct a thermosphere property under two opposing states (dayside maximum and nightside minimum) as EUV solar flux levels decrease. Under quiet geomagnetic conditions, the solar EUV flux is the major external driver of the thermosphere. This dayside source of energy drives a global neutral response that involves the redistribution of neutral mass, momentum, and thermal energy (as well as plasma effects).

The results of Section 5.2 indicate similarities between satellite observations and MSIS 2.0, while TIEGCM results display an opposing trend. A model-to-model comparison between MSIS 2.0 and TIEGCM output is warranted without the ambiguity introduced by the specific satellite sampling. Furthermore, other thermosphere properties can be investigated, like temperature, mean molecular weight, and pressure. Using the global nature of the models, the thermosphere properties are organized using the same selection criteria and averaging processes for each day of the 2002-2009 observing period. This allows for the generation of a timeseries without sampling gaps in our data and without the sampling-based arched structure seen in each precession window of the DNRs in the bottom panels of Figures 9 and 10. In this type of data gathering, the same criteria are used and all longitudes are averaged with respect to latitude.

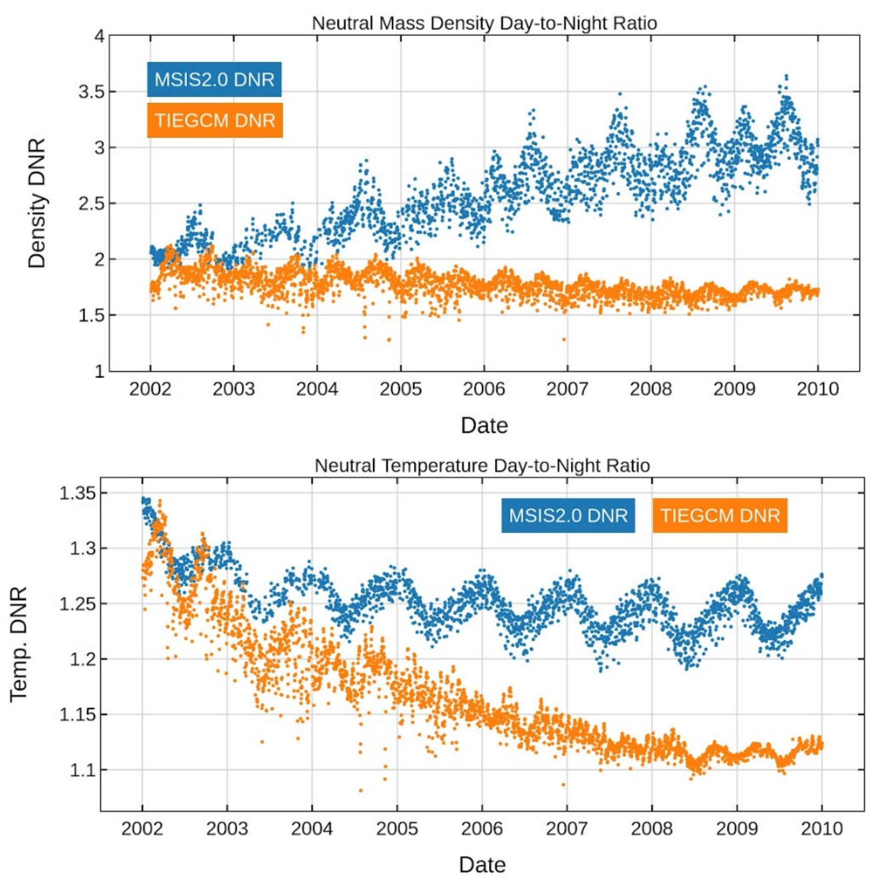

Figure 11. MSIS (blue) and TIEGCM (orange) day-to-night ratios for mass density (top) and temperature (bottom) at 400 km.

Figure 11 shows the comparison of DNRs for both density (Figure 11a) and temperature (Figure 11b) for the MSIS 2.0 and TIEGCM models. There is a semiannual pattern in the DNR for mass density and an annual pattern in the DNR for temperature, most prominently displayed by the MSIS 2.0 results. However, there are distinctly different climatological trends with solar flux between the two models that was first recognized in the satellite sampled DNR plots shown in Figure 10. The TIEGCM mass density DNR (orange) can now be clearly seen to decrease as solar flux decreases, while the MSIS 2.0 mass density DNR (blue) increases. The temperature DNRs also differ between models with the MSIS 2.0 showing little change with decreasing solar flux while the TIEGCM decreases.

The DNR captures the relative change between day and night values but does not indicate which value (dayside or nightside) is affecting the ratio and whether that is common among the models. The dayside density values between MSIS 2.0 and TIEGCM are similar for solar maximum, but MSIS 2.0 dayside densities exceed TIEGCM values when transitioning to solar minimum. The nightside MSIS 2.0 density values becoming increasing lower than the TIEGCM as solar flux decreases. A close inspection of the temperature values indicates that as the solar flux decreases the MSIS 2.0 temperatures are warmer on the dayside and cooler on the nightside with decreasing solar flux. These details help describe the differences in mass density and temperature DNR values displayed in Figure 11.

6 Discussion

The results of the data-model-model and model-model DNR comparisons indicate fundamental behavioral differences in how the two models represent the thermosphere during different levels of solar flux. It is difficult to reconcile the differences given the empirical and physics-based nature of the two models. Presumably MSIS 2.0 is close to representing the climatological behavior of the DNR values with changing solar flux due to its empirical construct – and this is supported by its agreeable comparison with the CHAMP data in Section 5.2. Thus, the TIEGCM must be misrepresenting physical processes that cause its simulated diurnal behavior in the neutral temperature and mass density to be off. Several studies using the TIEGCM have indicated issues in reconciling dayside and nightside behavior in neutral density and temperature. In developing a new data assimilation scheme for the TIEGCM, Sutton (2018) noted a persistent pattern in upper thermosphere neutral density of underprediction around noon/early afternoon and overprediction at night (i.e., a lower-than-expected DNR, similar to this study's finding). This was determined over a model interval of about 10-months in 2003 (high-to-medium solar flux). The paper concluded that such behavior is likely associated with the internal workings of the TIEGCM.

In the paper by Hsu et al. (2016), the TIEGCM was used to investigate the influence of drag forces - ion and viscous - on the wind and thermal structure of the upper thermosphere. A comparison was made between solar maximum and solar minimum. It clearly demonstrated that drag forces had a significant effect on the dayside and nightside thermal structure and that each drag force contributed differently depending on the level of solar flux. In solar maximum, ion drag forces were shown to be more dominant than viscous drag forces setting up a stronger thermal gradient between day and night (i.e., high-temperature DNR). During solar minimum, viscous drag forces dominated over ion drag forces. The role of viscosity, through momentum and energy coupling, lowered the dayside temperature and raised the nightside temperature (i.e., low-temperature DNR). These differing characteristics in drag forces indicated a dependency in solar flux that, if not adequately represented, can affect the temperature and density DNRs in the model. A deeper investigation into the inner workings of the TIEGCM is needed to explore the various dependencies of mass density and temperature response to solar flux.

To investigate contributing factors in producing the models' density DNR, DNR terms on the right-hand-side of Equation 7 in Section 2 are computed using MSIS 2.0 and TIEGCM V2.0 output. The DNR for a single day of model data is determined by averaging within the masking windows of latitude (±40°) and local time (dayside 11.5 - 17.5 LST, and nightside 23.5 - 5.5 LST) for a spectrum of EUV flux levels ranging from solar maximum ($F_{10.7}$=220) to solar minimum ($F_{10.7}$=80). Equation 7 is the ideal gas law expressed in terms of DNRs for the mean molecular weight, temperature, and pressure. The expression is applied to a fixed altitude of 400 km, $\rho_{DNR}^{400km} = \bar{m}_{DNR}^{400km} \frac{P_{DNR}^{400km}}{T_{DNR}^{400km}}$. Figure 12 presents dayside (top panels, solid lines), nightside (top panels, dashed lines), and DNR (bottom panels, solid) outputs from the two models for EUV flux levels ranging from solar maximum to solar minimum. Each data point along the plotted lines represents a model run where only the $F_{10.7}$ flux value is changed. The mean molecular weight and temperature panels in Figure 12 indicate the two models deviate in day and night values for both properties. The DNR values for the two properties, shown in the lower part of Figure 12, indicate similar values for solar maximum but diverging values at solar minimum. The sensitivity to solar flux levels in temperature DNR between the two models is similar to that seen in the multi-year simulation presented in Figure 11 in Section 5.3. In terms of sensitivity to solar flux, TIEGCM V2.0 temperature DNR values at 400 km show a stronger response to changing solar flux than MSIS 2.0. TIEGCM temperature DNR decreases toward one as solar flux decreases while MSIS 2.0 experiences only a small decrease in temperature DNR values – similar to Figure 11. TIEGCM

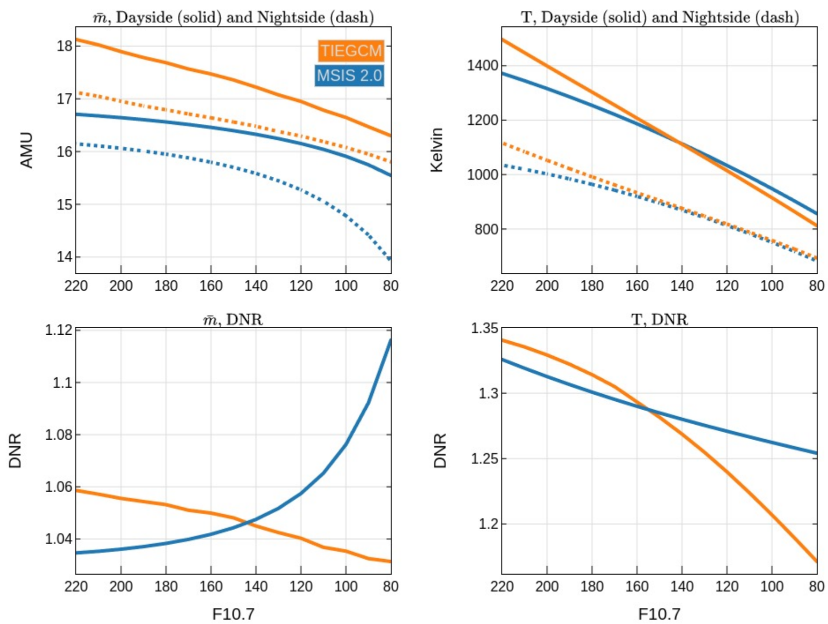

Figure 12. Top panels: Dayside (solid) and nightside (dashed) mean molecular weight (left) and temperature (right) at 400 km altitude from MSIS 2.0 (blue) and TIEGCM V2.0 (orange) for EUV flux levels ranging from solar maximum ($F_{10.7}$=220) to solar minimum ($F_{10.7}$=80). Lower panels: Mean molecular weight (left) and temperature (right) DNR values.

also tends to have mean molecular weight values at 400 km exceeding 16 AMU (i.e., more molecular nitrogen) while MSIS 2.0 values are often below 16 AMU, especially at solar minimum (i.e., more helium). MSIS 2.0 molecular weight DNR values at 400 km increase with decreasing solar flux while the TIEGCM V2.0 experiences little change – opposite to their relative temperature behavior. Thus, TIEGCM displays a greater sensitivity in temperature to solar flux while MSIS 2.0 displays a greater sensitivity in mean molecular weight to solar flux.

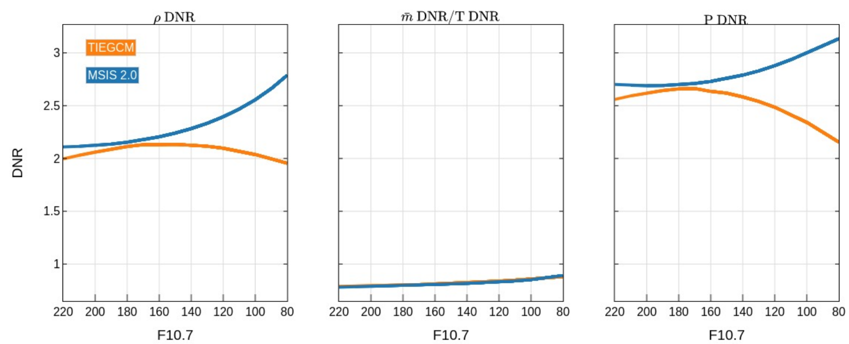

Figure 13. Terms of the DNR ideal gas equation from MSIS 2.0 (blue) and TIEGCM V2.0 (orange) across a range of EUV flux values from solar maximum to solar minimum.

In equation 7, the mean molecular weight DNR is divided by the temperature DNR. This result is plotted in Figure 13. Interestingly, the model differences exposed through the solar flux sensitivity analysis in Figure 12 cancel out to produce very similar outcomes between the two models. The two models agree when dividing the mean molecular weight DNR by the temperature DNR and this fractional value increases towards one as solar flux decreases in both models – this will be called the weighting factor in subsequent discussion.

The pressure DNR can also be calculated for each model and is shown in Figure 13. The pressure DNR from both models contribute the most to the density DNR value at 400 km. For solar maximum, the two models present similar pressure DNR values and weighting factors, resulting in mass density DNR values that are comparable – as determined in section 5.3. For solar minimum, we find distinctively different responses of the two models. As solar flux decreases the two models' estimate of pressure DNR deviate appreciably and trend in opposite directions. Given the weighting factor has no appreciable change between models, it can be concluded that the mass density DNR differences between MSIS 2.0 and TIEGCM V2.0 are related to the pressure DNR. The agreement in mass density DNR estimates between MSIS 2.0 and CHAMP observations suggests the trend in pressure DNR should be more like MSIS 2.0 than TIEGCM. The TIEGCM pressure relationship was described in section 2 and the pressure DNR is given as,

$$P_{DNR} = \exp\left(Z_{night} - Z_{day}\right) = \exp\left(\int_{h_0}^{h} \frac{dh}{H_{night}} - \int_{h_0}^{h} \frac{dh}{H_{day}}\right).$$

Thus, the pressure DNR is determined by the difference between inverse pressure scale heights for night and day. For discussion purposes, let's assume constant values in gravity and mean molecular weight throughout the upper thermosphere from 250 – 400 km for both models. Over this altitude range, the pressure scale height is then determined primarily by day and night exospheric temperatures (although composition can be influential in estimating scale height as altitude increases– see Liu et al. (2014)). Simply expressed,

$$P_{DNR} \approx \exp\left(\frac{\overline{m} g \Delta h}{k}\left(\frac{1}{T_\infty^N} - \frac{1}{T_\infty^D}\right)\right),$$

and using the exospheric temperature values from MSIS 2.0 and TIEGCM, the approximated pressure DNR values constitute more than 70% of the total pressure DNR values presented in Figure 13. Consequently, disparities between the models' density DNR at 400 km can largely be attributed to algebraic differences in their respective exospheric day and night temperatures, with a lesser influence by their differing mean molecular weight values. The integrative nature of the pressure DNR makes the mass density DNR very sensitive to composition and exospheric temperature differences between the two models for altitudes below 400 km. Using the results presented in Figure 12 for day and night exospheric temperature values, the TIEGCM nightside values are slightly warmer than MSIS 2.0, and the dayside TIEGCM temperatures around solar minimum are too cold. Increasing the dayside temperature values by about 50 – 100 K near solar minimum with a somewhat less decrease in night temperatures would bring the TIEGCM DNR values into better agreement with MSIS 2.0 and the observations. This agrees with the findings of Sutton (2018) and Hsu et al. (2016). Although only a 10% change in background exospheric temperature is necessary, the density response at 400 km can be of much greater percentage as it depends on the integrated effect of temperature below that altitude.

7 Conclusions

This paper introduces the use of day-to-night ratios of thermosphere properties as a metric for assessing how solar flux energy redistributes mass and thermal energy globally in the thermosphere. Eight years (2002-2009) of mass density data from processed CHAMP measurements were organized to elucidate relative changes in the dayside and nightside mass density at 400-km altitude over the changing solar flux. A CHAMP mass density day-to-night ratio (DNR) was computed in 3-degree latitude bins along every orbit and filtered based on specific criteria: equatorward of ±40 degrees latitude, Ap values < 15, dayside local solar times from 11.5 – 17.5, and nightside local solar times from 23.5 – 5.5. These criteria, combined with the satellite sampling and orbit precession, produced 29 DNR values per orbit and typically 60-day alternating intervals with and without DNR values due to orbit precession and local time constraints that shifted through seasons over the eight-year observing period. Solar flux decreased throughout the period beginning with $F_{10.7}$ values of about 200 and ending with values near 70. Over this decreasing solar flux, the CHAMP mass density DNR values demonstrated an increasing trend. This result differs from Müller et al. (2009) who found little dependence on solar flux over the CHAMP data set from 2002-2005. Presumably the detailed analysis and more extensive record used here has provided a more robust estimate demonstrating a clear increasing trend in mass density DNR with decreasing solar flux. This also illustrates that a near-constant value of about two, as suggested by (Müller et al., 2009) and (Qian & Solomon, 2012), is only appropriate near solar maximum and values more than four are observed during the declining phase of the solar cycle.

The MSIS 2.0 model was sampled along the CHAMP satellite orbit for an altitude of 400 km and processed with the same criteria to produce its own mass density DNR. The MSIS 2.0 mass density DNR values produced a similar trend as the CHAMP data with increasing DNR as the solar flux decreased. The TIEGCM V2.0 was run for the entire observing period and mass density values were interpolated to a 400 km altitude along the CHAMP satellite orbit. The model output was sampled in the same manner and used the same criteria to produce TIEGCM mass density DNRs. The TIEGCM results differed significantly from CHAMP and MSIS 2.0 with a decreasing mass density DNR with decreasing solar flux. The opposite trend in TIEGCM mass density DNR from observations indicates processes within the model are not reproducing the relative change in mass density between the dayside and nightside for decreasing solar flux values. This is a first-order effect in describing the thermosphere state and, although climatological, if the preconditioned state of the thermosphere is not properly represented it will influence how the system responds to a space weather event.

Due to the CHAMP results being reasonably represented by MSIS 2.0, the study investigated model-to-model differences in mass density and temperature DNRs without the CHAMP sampling and orbital effects that restricted the organization of the model output. The comparison between the two models illustrated a differing trend in both mass density and temperature DNRs at 400 km for decreasing solar flux. The TIEGCM temperature DNR decreased with decreasing solar flux while the MSIS 2.0 temperature DNR demonstrated only a minor decrease over the eight-year period. This difference in sensitivity to $F_{10.7}$ values was further illustrated by assessing the contributing factors of temperature, mean molecular weight, and pressure to mass density DNR. For MSIS 2.0, the mean molecular weight was more sensitive to changes in $F_{10.7}$, while the

TIEGCM displayed a greater sensitivity in temperature. Consequently, the two models deviated in their estimate of the pressure DNR at 400 km as solar flux decreased with MSIS 2.0 providing an appreciably higher value during solar minimum than TIEGCM V2.0. Model-model discrepancy in the pressure DNR is found to correlate extremely well with the overall mass density DNR differences. The pressure DNR is an integral function of both temperature and composition with height, of which we find temperature to be a more dominant contributor for this altitude. It was shown that disparities between the models' density DNR at 400 km can largely be attributed to algebraic differences in their respective exospheric day and night temperatures. The TIEGCM nightside values in exospheric temperature are slightly warmer than MSIS 2.0, but the dayside TIEGCM temperatures during middle-to-low solar flux are demonstrably too cold. Increasing the dayside temperature values by about 50 – 100 K during middle-to-low solar flux, with a somewhat less decrease in night temperatures, would bring the TIEGCM V2.0 DNR values into better agreement with MSIS 2.0 and the observations

The differing mass density trend with respect to solar flux revealed in the TIEGCM V2.0 output requires further investigation into the internal workings of the model under middle-to-low solar EUV flux levels. Solar insolation and heating efficiency within the model is one potential area of investigation. Another would concern how the global wind system sets up and how the various forces may change with solar flux levels altering thermal transport. Other feature differences, such as seasonal effects, are also evident in the model-to-model comparison but not investigated further in this study. This study has demonstrated that estimating a property's DNR is a useful metric to evaluate global thermosphere behavior. Observationally, the DNR is a relative metric that, by itself, does not indicate how each value contributes to the ratio but does help avoid the need for absolute calibration in its estimation from observations. It also provides the empirical evidence from which to test the models. From the model perspective, the DNR provides the means to evaluate the global response and the interconnectedness between dayside and nightside behavior in thermosphere properties. The DNR metric can be applied to other models to evaluate their thermosphere response to changing EUV flux.

Acknowledgments. This material is partially based upon work supported by the National Aeronautics and Space Administration under Grants #80NSSC21K1554 and #80NSSC20K1399 issued through the Heliophysics Division Space Weather Science Application initiative. The authors would also like to acknowledge the University of Colorado Space Weather Technology, Research and Education Center for its support and resources. There are no real or conceived financial conflict of interests for any author.

Open Research. The MSIS 2.0 model data, TIEGCM V2.0 simulation output, and CHAMP data used to generate the manuscript figures are available at Zenodo via doi:10.5281/zenodo.7255545. Jeffrey P. Thayer, Zachary C. Waldron, & Eric K. Sutton. (2022). Data archive accompanying "Solar Flux Dependence of Upper Thermosphere Diurnal Variations: Observed and Modeled". https://doi.org/10.5281/zenodo.7255546

References

Bruinsma, S., Tamagnan, D., & Biancale, R. (2004). Atmospheric densities derived from CHAMP/STAR accelerometer observations. *Planetary and Space Science*, *52*(4), 297–312. https://doi.org/10.1016/j.pss.2003.11.004

Dickinson, R. E., Lagos, C. P., & Newell, R. E. (1968). Dynamics of the neutral gas in the thermosphere for small Rossby number motions. *Journal of Geophysical Research (1896-1977)*, *73*(13), 4299–4313. https://doi.org/10.1029/JA073i013p04299

Doornbos, E., van den IJssel, J., Luhr, H., Forster, M., & Koppenwallner, G. (2010). Neutral Density and Crosswind Determination from Arbitrarily Oriented Multiaxis

Accelerometers on Satellites. *Journal of Spacecraft and Rockets*, *47*(4), 580–589. https://doi.org/10.2514/1.48114

Emmert, J. T. (2015). Thermospheric mass density: A review. *Advances in Space Research*, *56*(5), 773–824. https://doi.org/10.1016/j.asr.2015.05.038

Emmert, J. T., Drob, D. P., Picone, J. M., Siskind, D. E., Jones Jr., M., Mlynczak, M. G., et al. (2021). NRLMSIS 2.0: A Whole-Atmosphere Empirical Model of Temperature and Neutral Species Densities. *Earth and Space Science*, *8*(3), e2020EA001321. https://doi.org/10.1029/2020EA001321

Guo, J., Wan, W., Forbes, J. M., Sutton, E., Nerem, R. S., Woods, T. N., et al. (2007). Effects of solar variability on thermosphere density from CHAMP accelerometer data. *Journal of Geophysical Research: Space Physics*, *112*(A10). https://doi.org/10.1029/2007JA012409

Harris, I., & Priester, W. (1962). Time-Dependent Structure of the Upper Atmosphere. *Journal of the Atmospheric Sciences*, *19*(4), 286–301. https://doi.org/10.1175/1520-0469(1962)019<0286:TDSOTU>2.0.CO;2

Harris, I., & Priester, W. (1965). Of the Diurnal Variation of the Upper Atmosphere. *Journal of the Atmospheric Sciences*, *22*(1), 3–10. https://doi.org/10.1175/1520-0469(1965)022<0003:OTDVOT>2.0.CO;2

Hedin, A. E., Spencer, N. W., Mayr, H. G., Harris, I., & Porter, H. S. (1978). Direct evidence of transport processes in the thermospheric diurnal tide. *Journal of Geophysical Research: Space Physics*, *83*(A7), 3355–3357. https://doi.org/10.1029/JA083iA07p03355

Hsu, V. W., Thayer, J. P., Wang, W., & Burns, A. (2016). New insights into the complex interplay between drag forces and its thermospheric consequences. *Journal of Geophysical Research: Space Physics*, *121*(10). https://doi.org/10.1002/2016JA023058

Johnson, F. S., & Gottlieb, B. (1970). Eddy mixing and circulation at ionospheric levels. *Planetary and Space Science*, *18*(12), 1707–1718. https://doi.org/10.1016/0032-0633(70)90004-8

Kodikara, T., Carter, B., Norman, R., & Zhang, K. (2019). Density-Temperature Synchrony in the Hydrostatic Thermosphere. *Journal of Geophysical Research: Space Physics*, *124*(1), 674–699. https://doi.org/10.1029/2018JA025973

Lei, J., Thayer, J. P., & Forbes, J. M. (2010). Longitudinal and geomagnetic activity modulation of the equatorial thermosphere anomaly. *Journal of Geophysical Research: Space Physics*, *115*(A8), n/a-n/a. https://doi.org/10.1029/2009JA015177

Liu, X., Thayer, J. P., Burns, A., Wang, W., & Sutton, E. (2014). Altitude variations in the thermosphere mass density response to geomagnetic activity during the recent solar minimum. *Journal of Geophysical Research: Space Physics*, *119*(3), 2160–2177. https://doi.org/10.1002/2013JA019453

Mayr, H. G., & Harris, I. (1977). Diurnal variations in the thermosphere, 2. Temperature, composition, and winds. *Journal of Geophysical Research*, *82*(19), 2628–2640. https://doi.org/10.1029/JA082i019p02628

Mayr, H. G., & Volland, H. (1973). A two-component model of the diurnal variations in the thermospheric composition. *Journal of Atmospheric and Terrestrial Physics*, *35*(4), 669–680. https://doi.org/10.1016/0021-9169(73)90198-0

Müller, S., Lühr, H., & Rentz, S. (2009). Solar and magnetospheric forcing of the low latitude thermospheric mass density as observed by CHAMP. *Annales Geophysicae*, *27*(5), 2087–2099. https://doi.org/10.5194/angeo-27-2087-2009

Nicolet, M. (1961). Structure of the thermosphere. *Planetary and Space Science*, *5*(1), 1–32. https://doi.org/10.1016/0032-0633(61)90036-8

Qian, L., & Solomon, S. C. (2012). Thermospheric Density: An Overview of Temporal and Spatial Variations. *Space Science Reviews*, *168*(1), 147–173. https://doi.org/10.1007/s11214-011-9810-z

Qian, L., Burns, A. G., Emery, B. A., Foster, B., Lu, G., Maute, A., et al. (2014). The NCAR TIE-GCM (pp. 73–83). American Geophysical Union (AGU). https://doi.org/10.1002/9781118704417.ch7

Reber, C. A., & Hays, P. B. (1973). Thermospheric wind effects on the distribution of helium and argon in the Earth's upper atmosphere. *Journal of Geophysical Research (1896-1977)*, *78*(16), 2977–2991. https://doi.org/10.1029/JA078i016p02977

Solomon, S. C., Qian, L., Didkovsky, L. V., Viereck, R. A., & Woods, T. N. (2011). Causes of low thermospheric density during the 2007,Äì2009 solar minimum. *Journal of Geophysical Research: Space Physics (1978-2012)*, *116*(A2).

Stolle, C., & Liu, H. (2014). Low-Latitude Ionosphere and Thermosphere. In *Modeling the Ionosphere-Thermosphere System* (Vol. 9780875904917, pp. 259–272). Wiley Blackwell. https://doi.org/10.1002/9781118704417.ch21

Sutton, E. K. (2008). *Effects of Solar Disturbances on the Thermosphere Densities and Winds from CHAMP and GRACE Satellite Accelerometer Data*.

Sutton, E. K. (2009). Normalized force coefficients for satellites with elongated shapes. *Journal of Spacecraft and Rockets*, *46*(1), 112–116.

Sutton, E. K. (2016). Interhemispheric transport of light neutral species in the thermosphere. *Geophysical Research Letters*, *43*(24), 12,325-12,332. https://doi.org/10.1002/2016GL071679

Sutton, E. K. (2018). A New Method of Physics-Based Data Assimilation for the Quiet and Disturbed Thermosphere. *Space Weather*, *16*(6), 736–753. https://doi.org/10.1002/2017SW001785

Sutton, E. K., Nerem, R. S., & Forbes, J. M. (2007). Density and Winds in the Thermosphere Deduced from Accelerometer Data. *Journal of Spacecraft and Rockets*, *44*(6), 1210–1219. https://doi.org/10.2514/1.28641

Thuillier, G., & Bruinsma, S. (2001). The Mg II index for upper atmosphere modelling. *Annales Geophysicae*, *19*(2), 219–228. https://doi.org/10.5194/angeo-19-219-2001

Viereck, R. A., Floyd, L. E., Crane, P. C., Woods, T. N., Knapp, B. G., Rottman, G., et al. (2004). A composite Mg II index spanning from 1978 to 2003. *Space Weather*, *2*(10). https://doi.org/10.1029/2004SW000084

Volland, H. (1969). A theory of thermospheric dynamics-I. Diurnal and solar cycle variations. *Planetary and Space Science*, *17*(9), 1581–1597. https://doi.org/10.1016/0032-0633(69)90147-0